

An ultrahigh sensitivity, high resolution, aerostatic pressure sensor using microbubble resonators

Yong Yang(杨勇)^{1,2, a)} Sunny Saurabh,^{1, a)} Jonathan M Ward,¹ and Síle Nic Chormaic^{1, b)}

¹⁾ *Light-Matter Interactions Unit, Okinawa Institute of Science and Technology Graduate University, Onna, Okinawa 904-0495, Japan*

²⁾ *National Engineering Lab for Fiber Sensing Applications, Wuhan University of Technology, Wuhan, 430026, China*

(Dated: 25 July 2018)

Sensors based on whispering gallery resonators can push achievable sensitivities and resolutions to their limits, while maintaining minute footprints. Here, we report on the fabrication of a microbubble resonator using two CO₂ beams focused on a microcapillary; the resulting microbubble has an ultrathin wall. We show that, even when the wall is as thin as 500 nm, an intrinsic quality factor of 10⁷ is achievable at the telecommunications C-band. Considering strain and stress of the material, we investigate the feasibility of using the microbubble as an aerostatic pressure sensor. The measured sensitivity is 19 GHz/bar and is at the limit of current techniques. We have found that the sensitivity can be improved to 38 GHz/bar at the 780 nm wavelength range, where the resolution for pressure sensing is 0.14 mbar and the Q-factor remains higher than 10⁷.

Whispering gallery mode (WGM) microresonators (WGRs) have been used as high sensitivity sensors for many years. A wide variety of sensing applications have already been reported, such as temperature¹ and bio/chemical² sensing. With optical quality (Q) factors larger than 10⁵, WGM-based sensors usually have a high resolution. For example, the resolution for temperature sensing reached 2 mK in PDMS-coated microspheres¹. By utilizing the ultrahigh resolution of WGRs, single nanoparticle detection has also been demonstrated³.

Typically, WGRs are optically coupled using external optical waveguides. The resonator-waveguide system is then placed into the sensing environment, which is usually an aqueous solution. Ideally, the coupling waveguide should be isolated from this environmental fluid. For this purpose, a new WGR with a hollow structure was developed, the design of which is based on a microcapillary⁴. In contrast with solid WGRs, here the sensing occurs at the inner surface of the structure, while the WGMs can be excited by the external coupler via evanescent fields. For such structures, liquid can flow through the microcapillary and its properties, such as refractive index and viscosity, can be measured without disturbing the coupler (usually a tapered optical fiber). In general, there are two types of hollow structures, one of which is a microcapillary or bottle-like microcapillary, where the WGM is formed along the circumference of the capillary. The Q-factor can be ultrahigh; hence, in this kind of structure, optomechanical experiments, such as Brillouin scattering, can be performed⁵. Based on the optomechanics of hollow WGRs, sensing of liquid viscosity⁶ and aerostatic pressure⁷ have been implemented. If the wall of the resonator is reduced to less than the working wavelength the WGM is less confined and the Q-factor is

lower. Currently, the highest Q reported in this type of microresonator is less than 10⁵ for a wall thickness of 2 μm .⁸

The second type of hollow WGR is the microbubble^{9,10}. Geometrically, it is more like a microsphere on the outer surface, though it is hollow inside. Due to the curvature of the spherical shape, the mode is more confined in the polar direction compared with WGMs in microcapillary-based hollow resonators. Therefore, higher Q-factors can be achieved in thin-walled structures. Sensing applications have been reported in microbubble WGRs, such as strain⁹, refractive index¹¹ and bio/chemical sensing¹². Temperature sensing with a high resolution of 8.5 mK was realized in a thin-walled (submicron) microbubble filled with a liquid¹³. When the wall thickness is close to, or less than, the working wavelength of the WGM, certain modes are supported by the liquid contained in the microbubble; this is known as the *quasi-droplet regime*¹⁴. Here, the sensitivity is improved and, as a result, high resolution sensing is achievable, in principle. However, until now, the experimentally reported resolution is still lower than that for similar work in solid WGRs. In practice, the attainable Q-factor of microbubbles has not yet reached its upper bound due to radiation losses as a result of imperfections during the fabrication process.

In this paper, we present the latest progress on fabricating ultrathin-walled microbubbles with Q-factors greater than 10⁷ at the telecommunications C-band (around 1.55 μm). As a direct application, we measured the sensitivity of the WGM resonance frequency to the internal aerostatic pressure. Aerostatic tunability of microbubbles was first studied in 2011 by Henze *et al.*¹⁵ The applied inner pressure changes the microbubble's whispering gallery modes by two means: (i) a stress-induced refractive index change, dn/dp , which shifts the WGM frequency via an elasto-optical effect and (ii) a strain-induced size expansion, da/dp , which changes the total light path of the WGMs. Subsequently, we found

^{a)}Y. Y. and S. S contributed equally to this work.

^{b)}Electronic mail: sile.nicchormaic@oist.jp

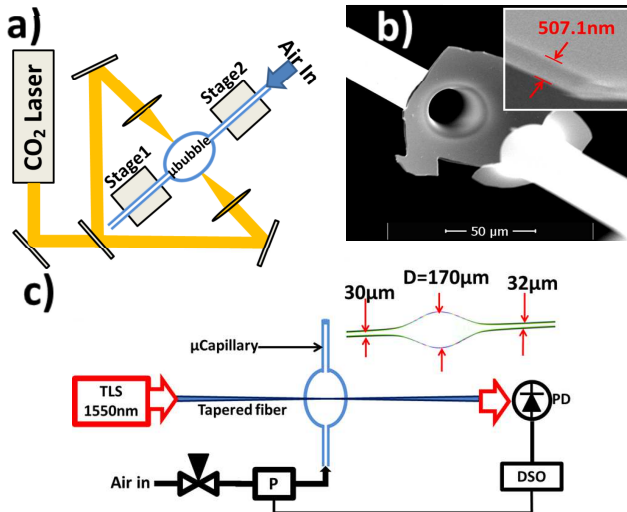


FIG. 1. (a) Schematic of the microbubble fabrication setup. (b) An SEM image of the microbubble snapped in the middle. The measured minimum wall thickness is 507 nm. (c) Experimental setup for aerostatic pressure sensing. P: electronic pressure sensor; PD: photon detector; DSO: digital oscilloscope.

that, for thin-walled microbubbles, the dominant effect is strain¹⁶. The frequency shift of the WGMs is linearly proportional to the internal pressure, while the sensitivity is proportional to a geometric parameter, χ . This geometric parameter is cubic to the radius of the microbubble and inversely cubic to the wall thickness. Therefore, in order to achieve high pressure sensitivity, the microbubble should be as large and thin-walled as possible. The pressure sensing resolution is, however, limited when the microbubble is too thin because, theoretically, the Q-factor drops exponentially with decreasing wall thickness. The rate of decrease is even faster in practice due to imperfections in the fabrication process. By improving the process, the theoretical Q-factor upper bound can be reached, therefore resulting in a high pressure sensing resolution.

A number of methods have been used for making thin-walled microbubbles. The overall requirement is to heat a small section of an internally pressurized capillary. When the glass softens, the applied gas pressure pushes the wall outwards to form a bubble or bottle shape. One method relies on heating a microcapillary with a rotating electric arc; in this way microbubbles with walls of 4 μm were made, with a reported Q-factor of 10^7 .¹⁷ A CO₂ laser can also be used for heating the microcapillary. By rotating the capillary in the focus of the CO₂ beam, a microbubble with a wall of 1 μm and a 10^6 Q-factor was obtained⁹. In the same way, a 560 nm walled microbubble with a diameter of 204 μm was later achieved for liquid lasing¹¹. The estimated Q of the lasing mode was 10^6 at 780 nm. Chemical etching can also be used to achieve a thin wall¹⁸.

In our work, instead of rotating the capillary or heater, we used two counterpropagating CO₂ laser beams focused on the capillary, as depicted in Fig.1(a). The crucial step to achieving an ultrathin microbubble was to use a silica capillary with a sufficiently small outer diameter and an inner-outer diameter ratio of 0.7 or greater. For example, in the setup described here, a capillary with an initial ID of 250 μm and OD of 350 μm was chosen and then pretapered down to an OD of around 30 μm . To taper the capillary, it was clamped on to two translation stages with the CO₂ laser focused on it. As the laser heated the capillary, one stage pulled the capillary out of the laser focus and the other stage fed the capillary into the focus at a much lower speed. This produced a thin microcapillary with a uniform waist at the required diameter. The microcapillary was next filled with compressed air and a microbubble was formed at the laser focus point. The expansion stops at a certain wall thickness, and, by increasing the laser power, larger, i.e. thinner, dual-input microbubbles can be formed. By controlling the power and heating time, a microbubble of diameter 170 μm and wall thickness about 507-570 nm (Fig.1(b)) was fabricated and used in the following experiments.

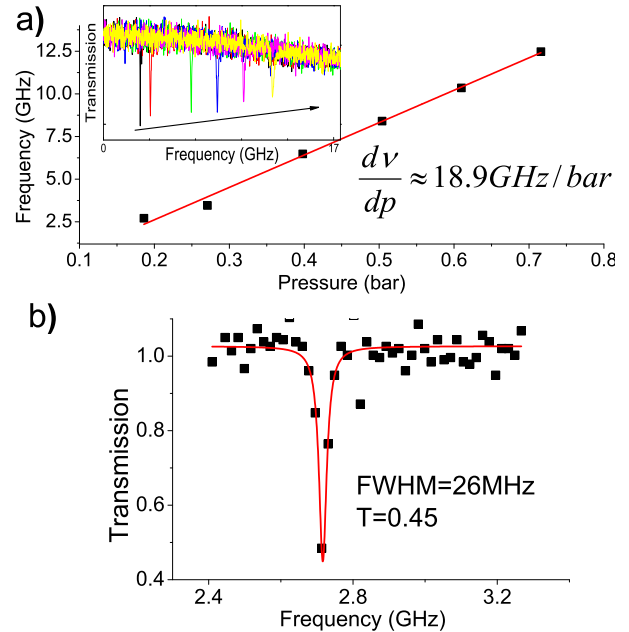


FIG. 2. (a) Pressure sensing sensitivity at 1.55 μm . The inset is the transmission spectrum, while increasing internal pressure. The arrow is the direction of the frequency shift. (b) Lorentz fitting of the transmission dip (left most curve on the inset of Fig 2(a)).

For pressure sensing, the dual-input microbubble was sealed at one end and connected to a pressure source at the other. The microbubble was then placed into an enclosure and, to maintain its high Q, it was purged with nitrogen gas. A high precision 3D nanopositioner was

used to determine the optimum, non-contact, evanescent coupling position with a tapered optical fiber. To measure the pressure sensitivity and Q-factor, a tunable laser at the 1550 nm band was scanned over a 17.5 GHz range and the transmission spectrum was recorded for different pressures (see Fig.1(c)).

Fig.2(a) is the relative frequency position of a specific mode for different inner pressures, fitted with a linear plot. The slope of the linear fit yields the sensitivity of this microbubble to be 19 GHz/bar. The linewidth of the transmission dip represents the loaded Q-factor of the system, shown in Fig.2(b). To compare with experimental results, the predicted sensitivity for a very thin-walled microbubble was determined from^{15,16}:

$$\frac{d\nu}{dp} \approx \frac{c}{\lambda^2} \left(\frac{3C}{n} + \frac{4G + 3K}{12GK} \right) \chi. \quad (1)$$

where c is the speed of light, n is the refractive index of silica, λ is the wavelength and ν is the frequency. In Eq.1, $\chi = b^3/(a^3 - b^3)$ with a and b representing the outer and inner radii. For silica, the opto-elasto coefficient $C = 4 \times 10^{-12} m^{-2}/N$, bulk modulus $G = 31 \times 10^9$ Pa and shear modulus $K = 41 \times 10^9$ Pa. The sensitivity from Eq.1 for different wall thicknesses and a diameter of 170 μm is plotted in Fig.3. Theoretically it is 21.5 GHz/bar for a wall thickness of 550 nm, which agrees with the experimental results.

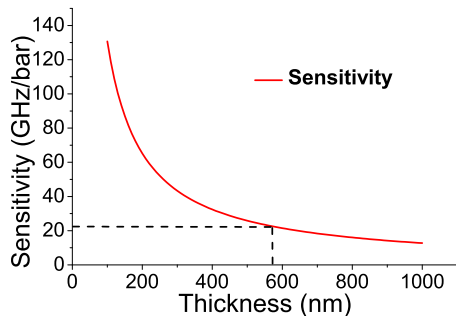


FIG. 3. Sensitivity calculated for different wall thickness at 1.55 μm and a microbubble diameter of 170 μm .

If we assume an ideal tapered fiber, undercoupled to the microbubble, the intrinsic Q can be deduced from the known transmission efficiency, T . From the data in Fig.2(b), the intrinsic Q is 9×10^6 . With a modified finite element method, the accurate Q-factor induced by the radiation and material losses can be simulated¹⁴(see Fig.4). At a wall thickness of 550 nm the simulation shows a Q-factor of 4.9×10^7 . Note that the model does not include losses from surface roughness or any contamination that may exist in practice. The measured Q is only 5 times smaller than the theoretical prediction. As a result, the resolution of the pressure sensing can be calculated on dividing the sensitivity by the linewidth, which yields a value of 1.3 mbar minimum at 1.55 μm .

To further improve the resolution and sensitivity, the measurements were repeated at 780 nm, shown in Fig.5.

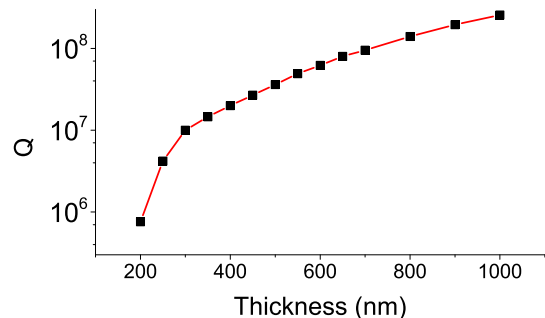


FIG. 4. Theoretical Q-factor of a 170 μm microbubble calculated for different wall thicknesses using a finite element method at 1.55 μm . The red line is a guide for the eye.

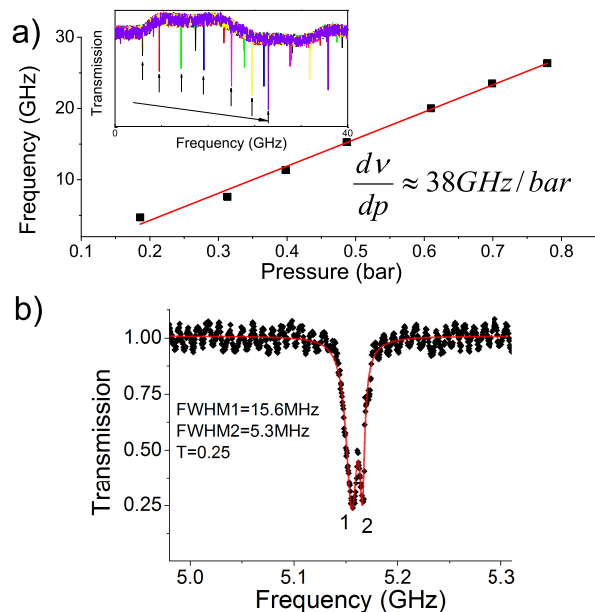


FIG. 5. (a) Pressure sensing sensitivity at 780 nm. The inset is the transmission spectrum, while increasing internal pressure. The arrow is the direction of the frequency shift.(b) Transmission dip used for determining the Q-factors of the microbubble modes.

From Eq.1, the sensitivity is related to wavelength. As a proof, the measured sensitivity from Fig.5(a) is 38 GHz/bar, which is twice that obtained at 1.55 μm . Also, for shorter wavelengths, the WGM light confinement is tighter, leading to a higher Q-factor. The measured transmission through the tapered fiber coupler is shown in Fig.5(b) and the observed double-peak structure occurs due to modal coupling. For each individual mode, the measured loaded Q-factors are 3.0×10^7 and 7.4×10^7 , respectively. Using the above method, the intrinsic Q-factors are 4.0×10^7 and 1×10^8 . Compared to the FEM simulation, which gives a Q-factor of 2×10^9 for a wall thickness of 550 nm, the obtained Q-factors are also close to the upper limit. Therefore, the resolution for the same

microbubble is increased to 0.14 mbar by using 780 nm light.

In summary, we have fabricated a submicron-walled microbubble with a high Q. Using this device, an ultra-high sensitivity aerostatic sensor was demonstrated, with a resolution of 0.14 mbar at 780 nm. This is not only useful for pressure sensing, but also other sensing applications. For 1.55 μm , a large evanescent field exists along the inner surface of the microbubble; this, together with the high Q property, could be used to detect single particles in air flow, as reported by Zhu *et al.*³ For the 780 nm wavelength range, when the 550 nm walled microbubble is filled with water, it operates in the quasi-droplet regime and this should be beneficial for index sensing¹⁴.

This work was supported by the Okinawa Institute of Science and Technology Graduate University. The authors thank B. Singh Bhardwaj for help in SEM imaging.

¹C.-H. Dong, L. He, Y.-F. Xiao, V. R. Gaddam, S. K. Ozdemir, Z.-F. Han, G.-C. Guo, and L. Yang, *Appl. Phys. Lett.* **94**, 231119 (2009).

²F. Vollmer and S. Arnold, *Nat. Methods* **5**, 591 (2008).

³J. Zhu, S. K. Ozdemir, Y.-F. Xiao, L. Li, L. He, D.-R. Chen, and L. Yang, *Nature Photon.* **4**, 46 (2009).

⁴J. Ward, N. Dhasmana, and S. Nic Chormaic, *Eur. Phys. J. Special Topics* **223**, 1917 (2014).

⁵G. Bahl, K. H. Kim, W. Lee, J. Liu, X. Fan, and T. Carmon, *Nature Commun.* **4**, 1994 (2013).

⁶K. Han, K. Zhu, and G. Bahl, *Appl. Phys. Lett.* **105**, 014103 (2014).

⁷K. Han, J. H. Kim, and G. Bahl, *Opt. Express* **22**, 1267 (2014).

⁸H. Li and X. Fan, *Appl. Phys. Lett.* **97**, 011105 (2010).

⁹M. Sumetsky, Y. Dulashko, and R. S. Windeler, *Opt. Lett.* **35**, 898 (2010).

¹⁰A. Watkins, J. Ward, Y. Wu, and S. Nic Chormaic, *Opt. Lett.* **36**, 2113 (2011).

¹¹W. Lee, Y. Sun, H. Li, K. Reddy, M. Sumetsky, and X. Fan, *Appl. Phys. Lett.* **99**, 091102 (2011).

¹²Y. Sun and X. Fan, *Anal. Bioanal. Chem.* **399**, 205 (2011).

¹³J. M. Ward, Y. Yang, and S. Nic Chormaic, *IEEE Photon. Tech. Lett.* **25**, 2350 (2013).

¹⁴Y. Yang, J. Ward, and S. Nic Chormaic, *Opt. Express* **22**, 6881 (2014).

¹⁵R. Henze, T. Seifert, J. Ward, and O. Benson, *Opt. Lett.* **36**, 4536 (2011).

¹⁶Y. Yang, S. Saurabh, J. M. Ward, and S. Nic Chormaic, *Opt. Lett.* **40**, 1834 (2015).

¹⁷S. Berneschi, D. Farnesi, F. Cosi, G. N. Conti, S. Pelli, G. C. Righini, and S. Soria, *Opt. Lett.* **36**, 3521 (2011).

¹⁸I. M. White, H. Oveys, and X. Fan, *Opt. Lett.* **31**, 1319 (2006).